Technical Note

Application of the Rossiter Model for Predicting the Frequency of Vortex Shedding and Surface Oscillations in Rectangular Shallow Reservoirs

Emmanuel Mignot[1] and Benjamin Dewals[2]

Abstract: Shallow reservoirs are ubiquitous in hydraulic engineering. Predicting the properties of the flow field in such reservoirs is instrumental to inform their design, operation, and maintenance. In previous research, oscillating jets were experimentally observed in rectangular shallow reservoirs, and we assess here the performance of a simple analytical model to predict the frequency of the dominating jet oscillation mode(s). The model couples the evaluation of the reservoir natural frequencies with the Rossiter feedback loop formula. The analytical predictions are compared against experimental observations by reanalyzing an existing data set. In many cases, the model predictions match the observations. Remaining discrepancies may result from experimental uncertainties, which could be reduced in future tailored laboratory tests, or from the dimensionless vortex celerity value used by the feedback loop model, which was not assessed experimentally. **DOI: 10.1061/JHEND8.HYENG-13929.** © *2024 American Society of Civil Engineers.*

Introduction

Shallow reservoirs are common hydraulic structures serving multiple purposes. They are used for stormwater management (Dufresne et al. 2009; Adamsson et al. 2003) and wastewater treatment (Izdori et al. 2019), as service reservoirs in water supply systems (Zhang et al. 2014), as constructed wetlands (Guzman et al. 2018; Persson and Wittgren 2003), or as settling basins (Lakzian et al. 2020; Liu et al. 2013). Many of these reservoirs are rectangular or closely approximate this shape (Dufresne et al. 2009; Li and Sansalone 2021; Liu et al. 2013; Tarpagkou and Pantokratoras 2013; Zhang et al. 2014). Designing, operating, and maintaining these reservoirs is challenging. Minimizing sedimentation is crucial for storage facilities, while maximizing it is essential for sedimentation tanks. For example, efficient sediment trapping in stormwater reservoirs significantly affects the water quality (Guzman et al. 2018). Predicting sediment deposition patterns is essential for planning maintenance of storage facilities (Izdori et al. 2019).

Numerous experimental studies have examined the flow fields developing in rectangular shallow reservoirs, unveiling complex hydrodynamic processes despite the simple geometry (Adamsson et al. 2003; Camnasio et al. 2011; Dewals et al. 2008; Dufresne et al. 2009, 2010a; Peltier et al. 2014a). Depending on the reservoir aspect ratio and the hydraulic boundary conditions, distinct flow patterns were observed. For rectangular reservoirs with aligned central inlet and outlet channels, the flow field may involve a detached jet, a reattached jet, or a meandering jet (Miozzi and Romano 2020; Peltier et al. 2014a, b). Sediment trapping and mixing efficiency vary significantly between these flow patterns (Adamsson et al. 2003; Camnasio et al. 2013; Dufresne et al. 2009, 2010b; Yan et al. 2020). Therefore, accurately predicting the flow field is crucial in engineering applications. Here, we investigate the potential to predict the oscillation frequency of a meandering jet in such a rectangular shallow reservoir with aligned central inflow and outflow channels.

The prediction of the peak oscillation frequency of a monophasic jet impinging a wall or the mixing layer at the interface between a semienclosed cavity and a mainstream has been performed for about 60 years (Table 1) using the so-called feedback loop formula, introduced by Rossiter (1964). This method is not predictive because several solutions exist for a given flow configuration (Heller et al. 1971). Therefore, Kegerise (1999) coupled the Rossiter formula with the calculation of the natural frequencies of the fluid domain to make the coupled model semipredictive. Perrot-Minot et al. (2020) recently adapted this coupled model to an open-channel configuration. The authors were able to predict the peak oscillating frequency of the mixing layer at the interface between a lateral isolated cavity and the adjacent mainstream. This frequency is equal to that of the vortex shedding along the mixing layer and that of the free-surface oscillations in the basin. For the feedback loop model to apply, two ingredients are required: a vortex street (along which vortices travel one after the other) and a downstream wall in the alignment of the vortex street where the vortices impinge. Fig. 1 lists five geometrical configurations typically encountered in natural or human-made, riverine or urban water environments, for which the feedback loop formula could be applied to predict the vortex shedding frequency. Apart from the lateral cavity already considered by Perrot-Minot et al. (2020) [as sketched in Fig. 1(a)], the other configurations are a reservoir [Fig. 1(b)], a groyne field [Fig. 1(c)], a sediment trap [Fig. 1(d)], and the space between consecutive macroroughness elements [Fig. 1(e)]. This list is certainly not exhaustive.

The aim of the present work is to assess the validity of the coupled model for the meandering jet at the center of a shallow reservoir, as shown in Fig. 1(b). Given the comprehensive data set of meandering jet configurations provided by Peltier et al. (2014a), including measured oscillating frequencies, their observations were

[1]Associate Professor, Laboratoire de Mécanique des Fluides et Acoustique (LMFA), Institut National des Sciences Appliquées (INSA) Lyon, Ecole Centrale de Lyon (ECL), Centre Nationale de Recherche Scientifique (CNRS), Université Claude Bernard Lyon 1, Villeurbanne 69621, France (corresponding author). ORCID: https://orcid.org/0000-0002-4894-2254. Email: Emmanuel.mignot@insa-lyon.fr

[2]Professor, Hydraulics in Environmental and Civil Engineering, Univ. of Liège, Liège 94000, Belgium. Email: b.dewals@uliege.be

Note. This manuscript was submitted on September 27, 2023; approved on June 10, 2024; published online on August 28, 2024. Discussion period open until January 28, 2025; separate discussions must be submitted for individual papers. This technical note is part of the ***Journal of Hydraulic Engineering***, © ASCE, ISSN 0733-9429.

Table 1. Literature review of the application of the feedback loop formula with the corresponding measured or selected ratio of vortex celerity (c_v) to the mean flow velocity (U)

Configuration	Reference	c_v/U
Impinging jets (in air)	Ho and Nosseir (1981)	0.62
	Tam et al. (1986)	0.7
	Powell et al. (1992)	0.64–0.75
	Panda (1999)	0.68–0.7
	Gao and Li (2010)	0.57–0.74
	Mercier et al. (2017)	0.54–0.61
Cavity (in air)	Rossiter (1964)	0.57
	East (1966)	0.35–0.6
	Block (1976)	0.57
	Ahuja and Mendoza (1995)	0.65
	Colonius et al. (1999)	0.57
	Larchevêque et al. (2003)	0.38–0.62
	Rowley et al. (2006)	0.625
Open-channel cavity	Perrot-Minot et al. (2020)	0.56

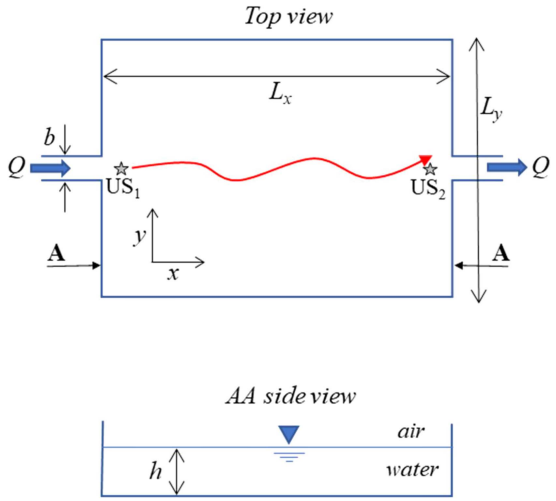

Fig. 2. Rectangular shallow reservoir considered by Peltier et al. (2014a).

reanalyzed here and used as a reference for assessing the performance of the coupled model.

The paper is organized as follows. The first section presents the experimental procedure and the list of flow configurations. Both ingredients of the analytical model are then presented: first the calculation of the reservoir natural frequencies and then the Rossiter feedback loop formula. Finally, the predicted and measured frequencies are compared to assess the reliability of the model.

Data and Methods

Laboratory Experiments

Peltier et al. (2014a) performed laboratory experiments to characterize the flow field in a horizontal, smooth, rectangular shallow reservoir with one narrow inlet at the center of the upstream wall and one outlet of same width at the center of the downstream wall (Fig. 2). In a series of tests, the authors kept the reservoir width (L_y) and length (L_x) constant, with $L_y = 0.985$ m and $L_x = 1$ m. Two different inlet channel widths b were considered ($b = 0.06$ and 0.08 m). The inlet discharge Q (adjusted by a valve in the pumping loop and measured with an electromagnetic flowmeter) and the water depth h (adjusted by a downstream tailgate) were independently varied to generate a large set of flow configurations. A meandering jet was observed in 26 configurations, which are considered herein. The corresponding hydraulic conditions, including the flow discharge Q, mean water depth h, and corresponding Froude number F, are detailed in Table 2.

The free-surface velocity field in the reservoir was measured by Peltier et al. (2014a) with a large scale particle image velocimetry (LSPIV) method at a recording rate of 25 frames per second during more than 7 min over an area of about 1×1 m with a final spatial resolution of 1 mm per pixel, e.g., about 1,000 pixels over the length and width of the reservoir. By applying a proper orthogonal decomposition (POD) of the velocity field, Peltier et al. (2014a) obtained the oscillation frequency of the most energetic modes of the impinging jet. The frequency of the first pair of modes is

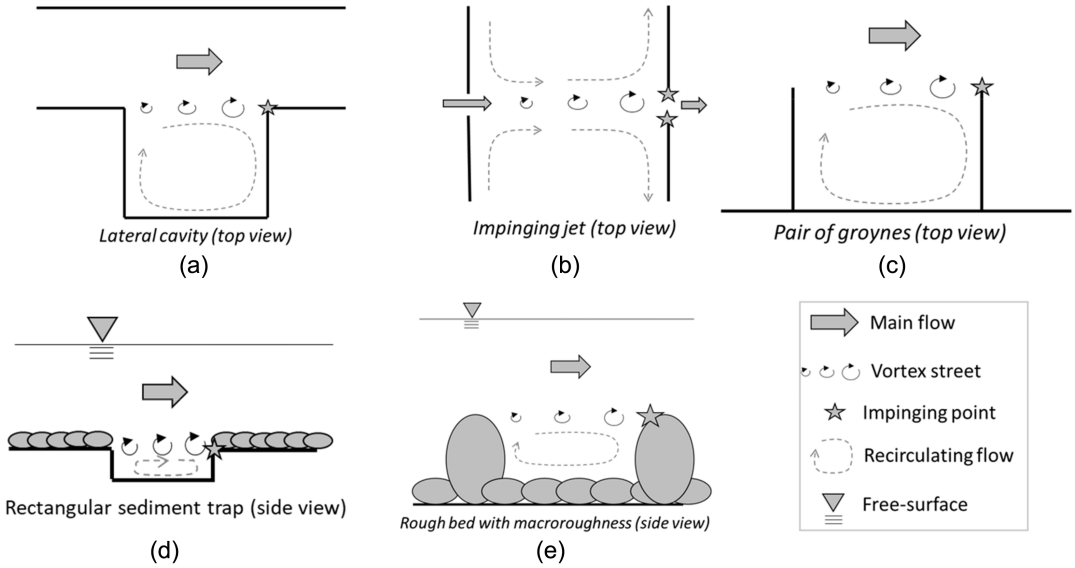

Fig. 1. Examples of geometrical configurations in the riverine environment to which the present Rossiter model (a) was applied by Perrot-Minot et al. (2020); (b) is applied in the present research; or (c–e) could be applied in future works.

Table 2. Characteristics of the tested configurations along with the measured peak frequencies

L_x (m)	L_y (m)	b (m)	h (cm)	Q (L/s)	F	f_{vel} (Hz)	f_{US} (Hz)
1	0.985	0.08	1.80	0.25	0.41	0.228	0.220
			2.74	0.50	0.44	0.259	0.269
			5.56	1.53	0.47	0.509	0.391 0.537
			1.25	0.13	0.36	0.172	?
			1.95	0.12	0.18	0.197	?
			2.24	0.26	0.31	0.270	?
			2.90	0.50	0.40	0.263	0.269
			4.23	1.00	0.46	0.476	0.342 0.464
			5.40	1.46	0.46	0.557	0.391 0.537
			5.84	1.43	0.40	0.447	0.391
			4.96	1.03	0.37	0.369	0.350
			3.78	0.48	0.26	0.317	0.317
			3.27	0.24	0.16	0.061	?
		0.06	3.39	0.50	0.42	0.275	0.293
			2.10	0.25	0.44	0.229	?
			1.41	0.13	0.41	0.233	?
			5.19	1.01	0.45	0.514	0.366 0.513
			2.12	0.13	0.22	0.246	?
			2.55	0.27	0.35	0.259	?
			3.44	0.50	0.41	0.280	0.293
			5.06	0.98	0.46	0.378	0.366
			6.69	1.50	0.46	0.412	0.415 0.586
			6.84	1.48	0.44	0.418	0.415
			5.59	1.00	0.40	0.364	0.366
			4.04	0.51	0.33	0.423	?
			3.24	0.25	0.22	0.293	?

noted f_{vel} in Table 2, where subscript vel stands for velocity measurements. These frequencies were previously compared against the predictions of a two-dimensional shallow-water model by Peltier et al. (2015).

Two water depth signals were recorded with ultrasonic sensors (uncertainty of 0.2 mm) located above the reservoir, near the inlet (US_1) and outlet (US_2) channels, as depicted in Fig. 2. Each measurement lasted 122 s with a sampling frequency of 50 Hz, corresponding to 6,100 sampling points. Detecting the peak values of the Welch spectra applied on these signals allowed us to estimate the peak frequency (noted f_{US}) of the free-surface oscillations. In some cases, the amplitude of free-surface oscillations was too low to enable detecting a distinctive peak in the spectra, and these cases are labeled with question marks in Table 2. Conversely, in some configurations, two peaks were identified, indicating a bidirectional seiching (Engelen et al. 2020) and the two values are reported in Table 2.

As shown in Fig. 3, the peak frequencies obtained by both methods match very well. This suggests that the same peak frequencies govern the oscillating jet and the free-surface oscillation, as described by Perrot-Minot et al. (2020) in an isolated lateral open-channel cavity.

Natural Frequencies of the Reservoirs

Following Rabinovitch (2009), the natural frequencies $f_{n_x n_y}$ of a rectangular open-channel basin are computed as

$$f_{n_x n_y} = \frac{c_g}{2}\left[\left(\frac{n_x}{L_x}\right)^2 + \left(\frac{n_y}{L_y}\right)^2\right]^{1/2} \quad (1)$$

where n_x and n_y = number of nodes of the corresponding mode along, respectively, the x- and y-directions; L_x and L_y = characteristic dimensions along each direction (Fig. 2); and c_g = celerity of the gravity waves computed as follows (Lamb 1945):

$$c_g = \frac{g}{2\pi f}\tanh\left(\frac{2\pi h f}{c_g}\right) \quad (2)$$

with g = gravity acceleration.

Perrot-Minot et al. (2020) proposed to normalize the natural frequencies by the frequency f_{10} of the first streamwise oriented natural mode (with a single node along x-axis). Eq. (1) thus reads

$$\frac{f_{n_x n_y}}{f_{10}} = \left[n_x^2 + \left(\frac{n_y}{L_y/L_x}\right)^2\right]^{1/2} \quad (3)$$

Because L_x and L_y are kept constant in the present data set (Table 2), the nondimensional natural frequencies remain the same for all configurations. The first three values (with n_x and $n_y \leq 1$) are plotted in Fig. 4 as a function of F; they appear as horizontal dashed lines. Moreover, because in the present work the aspect ratio of the reservoir is close to unity ($L_y/L_x = 0.985$), $f_{n_x n_y} \approx f_{n_y n_x}$ so that $f_{01} \approx f_{10}$.

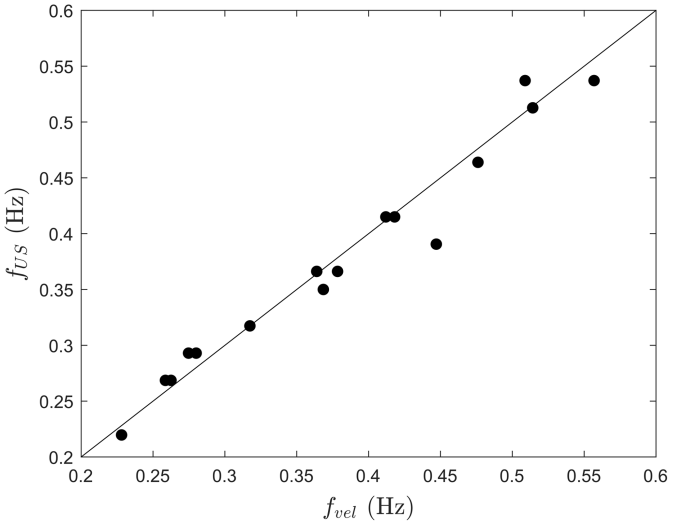

Fig. 3. Comparison of the peak frequencies measured by LSPIV and POD (f_{vel}) and by the ultrasonic sensors (f_{US}), when available (Table 2).

Feedback Loop Formula

As a vortex is shed at the upstream extremity of the jet, i.e., at the outlet of the inlet channel, it travels at a celerity noted c_v (where v stands for vortex) along the jet toward the downstream wall. As the vortex impinges the wall, a gravity wave is generated and propagates with a celerity c_g [Eq. (2)] in all directions, including the direction back toward the jet upstream end where the gravity wave interacts with the vortex shedding process. The feedback loop formula is based on two assumptions: (1) that both processes have the same frequency, and (2) that both waves are in phase at the jet upstream and downstream ends. These assumptions are supported by the fact that the impinging jet generates the gravity wave at the downstream wall and that the gravity wave triggers the vortex shedding at the jet entrance. This implies that the time taken by a vortex to travel all along the jet from upstream to downstream (equal to L_x/c_v) added to the time taken by the gravity wave to travel back from the impinging wall to the jet entrance

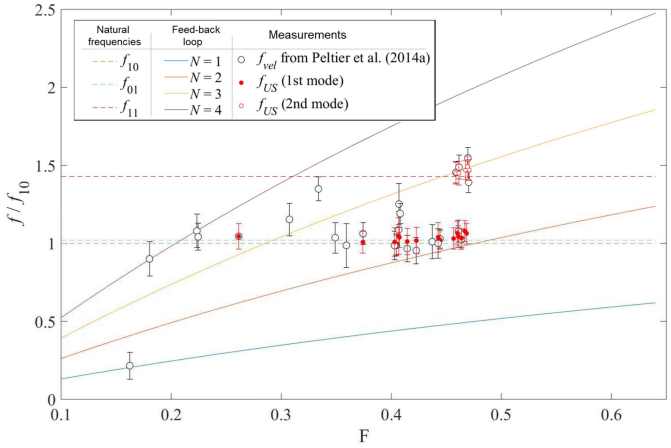

Fig. 4. Comparison between the coupled model and the measured data.

(equal to L_x/c_g) must be a multiple number (N) of periods of the feedback loop (or to the inverse of its frequency noted f_N), so that

$$\frac{L_x}{c_v}+\frac{L_x}{c_g}=\frac{N}{f_N} \tag{4}$$

As derived by Perrot-Minot et al. (2020), the mathematical expression of the feedback loop formula then reads

$$f_N=\frac{N}{\frac{L_x}{c_v}+\frac{L_x}{c_g}} \tag{5}$$

where f_N = vortex shedding frequency, equal to the jet oscillating peak frequency; and N = positive integer ($N=1,2,\ldots$). As for the natural frequencies [Eq. (3)], the feedback loop frequency can be normalized by the first streamwise natural frequency f_{10} as follows:

$$\frac{f_N}{f_{10}}=\frac{1}{\frac{c_g}{2L_x}\frac{L_x}{c_v}+\frac{L_x}{c_g}}=\frac{2N\mathrm{F}}{\frac{U}{c_v}+\mathrm{F}} \tag{6}$$

where $U=Q/(bh)$ is the flow velocity in the inlet channel; and $\mathrm{F}=U/c_g$ is the corresponding Froude number.

For a given configuration from Table 2, all parameters from Eq. (6) are known except for the vortex advection celerity c_v. Peltier et al. (2014a) did not measure c_v, but empirical estimates of the ratio of c_v to U are available in the literature (Table 1). The ratio used herein is an average of the value reported for impinging jets (in air): $c_v/U=0.70$. The solutions of Eq. (6) for $N\leq 4$ are plotted in Fig. 4 as a function of F, where they appear as monotonically increasing curves.

Normalization of Experimentally Observed Frequencies

Consistently with Eqs. (3) and (6), the measured peak frequencies are normalized by f_{10} and read

$$\frac{f}{f_{10}}=\frac{f}{\frac{c_g}{2}\frac{1}{L_x}}=\frac{2fL}{c_g} \tag{7}$$

The normalized peak frequencies measured with LSPIV (f_{vel}/f_{10}) and with the ultrasonic sensors (f_{US}/f_{10}) are finally added to Fig. 4 as symbols.

Results

Identification of Measured Natural Frequencies

Most measured peak frequencies (f_{vel} or f_{US}) in Fig. 4 appear to be close to a natural frequency of the shallow reservoir (i.e., most symbols are located on, or relatively close to, a horizontal line). For the 26 configurations tested herein, 21 exhibit a peak frequency equal to f_{10} (along the x-axis) or f_{01} (along the y-axis), among which five also exhibit a f_{11} second peak frequency [and are thus in bidirectional seiching, with two dominating modes, see Engelen et al. (2020)].

In the two configurations with the lowest Froude number ($\mathrm{F}<0.2$), the measured frequency differs from any natural frequency. This is also the case for three other configurations with a larger Froude number but the currently available data (Peltier et al. 2014a), which were not collected for the purpose of the present study, do not enable pointing at a clear-cut explanation for this deviation.

Application of the Coupled Model

The coupled model (natural frequency and feedback loop formula) assumes that, for a given configuration, the peak frequency equals the frequency that best fits both a natural frequency and a solution of the feedback loop formula. Graphically, this coupling results in selecting the natural frequency located the closest to an intersection between a horizontal line (natural frequency) and a monotonically increasing curve corresponding to a specific N value (solution of the feedback loop formula).

For example, the coupled model predicts that for $\mathrm{F}=0.2$, $f=f_{01}$ or $f=f_{10}$ and $N=4$ as two intersections are observed for $\mathrm{F}\approx 0.2$: f_{01} and $N=4$, as well as f_{10} and $N=4$. The agreement of these predictions with the measured frequencies for the two flow configurations with $\mathrm{F}\approx 0.22$ (Fig. 4) supports the validity of the coupled model. As another example, for $\mathrm{F}\approx 0.45$–0.47, three intersections are observed: $f=f_{11}$ and $N=3$, as well as $f=f_{10}$ or f_{01} and $N=2$. Fig. 4 shows that for all configurations with $0.45<\mathrm{F}<0.5$ (except one), two peak frequencies were indeed measured, one about equal to f_{01} or f_{10}, and the second about equal to f_{11}.These data are also consistent with the predictions of the coupled model. The fair agreement between the predicted and measured peak frequencies suggests that the coupling between a natural mode and the feedback loop is indeed the physical mechanism controlling the jet meandering frequency.

In contrast, for $\mathrm{F}\approx 0.3$, three intersections can be observed at $f=f_{11}$ and $N=4$, as well as at $f=f_{01}$ or f_{10} and $N=3$. However, the peak frequency for the configuration with $\mathrm{F}=0.31$ is measured at an intermediate value between these intersections. This discrepancy between the predicted and measured peak frequencies remains unclear from the currently available experimental data. Unfortunately, no ultrasonic sensor frequency peak (f_{US}) could be estimated for this configuration to assess the validity of the measured POD peak frequency (f_{vel}).

Besides, for $0.35<\mathrm{F}<0.4$, no intersection exists in Fig. 4. However, the majority of frequencies measured within this range correspond to a natural frequency of the reservoir with a single node (f_{01} or f_{10}). Similarly, no intersection exists for $\mathrm{F}<0.2$. For these configurations the measured peak frequency differs from any natural frequency, but they match a solution of the feedback loop Rossiter formula with $N=1$ for $\mathrm{F}=0.16$ and $N=4$ for $\mathrm{F}=0.18$.

Conclusion

The present work aimed at assessing the capacity of the model coupling the Rossiter feedback loop formula and the natural frequency of the reservoir to predict the peak frequencies of the meandering jet at the center of a shallow reservoir impinging the downstream wall. The model was evaluated based on a set of 26 flow configurations measured in a rectangular reservoir with an aspect ratio close to 1. The results confirm that most measured peak frequencies are equal to a natural frequency of the shallow reservoir and are equal to the closest intersection between the natural frequency curves and the solutions of the feedback loop formula. Still, a few measured frequencies seem to differ from the predicted ones. The discrepancies between present measurements and model predictions may originate from the experimental data precision or from the model validity. Regarding the experimental data, the ultrasonic (water level) measurements from Peltier et al. (2014a) last only 2 min (at a sampling rate of 50 Hz), while Perrot-Minot et al. (2020) used a 10-min series of ultrasonic measurements (at a sampling rate of 200 Hz). Peltier et al.'s (2014a) data are thus expected to be of lower precision. Regarding the feedback loop model, the main unknown is the value of the vortex advection celerity c_v, taken here as $c_v/U = 0.7$ as proposed by the aeroacoustics literature on impinging jets, without specific experimental validation for free-surface reservoirs [unlike in the case of the cavity configuration where this ratio was experimentally adjusted by Perrot-Minot et al. (2020)]. In future experiments, it would be valuable to better capture the spatial distribution of the free-surface oscillations [as performed by Perrot-Minot et al. (2020)] to enable discriminating between the various possible modes. Another inherent limitation of the coupled model is that it is not fully predictive in the sense that, for some configurations, several close intersections exist, and the model does not permit predicting which one will actually be occurring.

Data Availability Statement

All data, models, and code generated or used during the study appear in the published article.

References

Adamsson, Å., V. Stovin, and L. Bergdahl. 2003. "Bed shear stress boundary condition for storage tank sedimentation." *J. Environ. Eng.* 129 (Jan): 651–658. https://doi.org/10.1061/(ASCE)0733-9372(2003)129:7(651).

Ahuja, K. K., and J. Mendoza. 1995. *Effects of cavity dimensions, boundary layer, and temperature on cavity noise with emphasis on benchmark data to validate computational aeroacoustic codes*. NASA Contractor Rep. No. 4653. Hampton, VA: National Aeronautics and Space Administration, Langley Research Center.

Block, P. J. 1976. *Noise response of cavities of varying dimensions at subsonic speeds*. NASA Technical Notes, D-8361. Hampton, VA: National Aeronautics and Space Administration, Langley Research Center.

Camnasio, E., S. Erpicum, E. Orsi, M. Pirotton, A. J. Schleiss, and B. Dewals. 2013. "Coupling between flow and sediment deposition in rectangular shallow reservoirs." *J. Hydraul. Res.* 51 (5): 535–547. https://doi.org/10.1080/00221686.2013.805311.

Camnasio, E., E. Orsi, and A. J. Schleiss. 2011. "Experimental study of velocity fields in rectangular shallow reservoirs." *J. Hydraul. Res.* 49 (3): 352–358. https://doi.org/10.1080/00221686.2011.574387.

Colonius, T., A. Basu, and C. Rowley. 1999. "Numerical investigation of the flow past a cavity." In *Proc., 5th AIAA/CEAS Aeroacoustics Conf. and Exhibit*. Reston, VA: American Institute of Aeronautics and Astronautics.

Dewals, B. J., S. A. Kantoush, S. Erpicum, M. Pirotton, and A. J. Schleiss. 2008. "Experimental and numerical analysis of flow instabilities in rectangular shallow basins." *Environ. Fluid Mech.* 8 (1): 31–54. https://doi.org/10.1007/s10652-008-9053-z.

Dufresne, M., B. J. Dewals, S. Erpicum, P. Archambeau, and M. Pirotton. 2010a. "Classification of flow patterns in rectangular shallow reservoirs." *J. Hydraul. Res.* 48 (2): 197–204. https://doi.org/10.1080/00221681003704236.

Dufresne, M., B. J. Dewals, S. Erpicum, P. Archambeau, and M. Pirotton. 2010b. "Experimental investigation of flow pattern and sediment deposition in rectangular shallow reservoirs." *Int. J. Sediment Res.* 25 (3): 258–270. https://doi.org/10.1016/S1001-6279(10)60043-1.

Dufresne, M., J. Vazquez, A. Terfous, A. Ghenaim, and J. B. Poulet. 2009. "Experimental investigation and CFD modelling of flow, sedimentation, and solids separation in a combined sewer detention tank." *Comput. Fluids* 38 (5): 1042–1049. https://doi.org/10.1016/j.compfluid.2008.01.011.

East, L. F. 1966. "Aerodynamically induced resonance in rectangular cavities." *J. Sound Vib.* 3 (3): 277–287. https://doi.org/10.1016/0022-460X(66)90096-4.

Engelen, L., C. Perrot-Minot, E. Mignot, N. Riviere, and T. De Mulder. 2020. "Experimental study of bidirectional seiching in an open-channel, lateral cavity in the time and frequency domain." *Phys. Rev. Fluids* 5 (10): 104801. https://doi.org/10.1103/PhysRevFluids.5.104801.

Gao, J. H., and X. D. Li. 2010. "A multi-mode screech frequency prediction formula for circular supersonic jets." *J. Acoust. Soc. Am.* 127 (3): 1251–1257. https://doi.org/10.1121/1.3291001.

Guzman, C. B., S. Cohen, M. Xavier, T. Swingle, W. Qiu, and H. Nepf. 2018. "Island topographies to reduce short-circuiting in stormwater detention ponds and treatment wetlands." *Ecol. Eng.* 117 (Sep): 182–193. https://doi.org/10.1016/j.ecoleng.2018.02.020.

Heller, H. H., D. G. Holmes, and E. E. Covert. 1971. "Flow-induced pressure oscillations in shallow cavities." *J. Sound Vib.* 18 (4): 545–553. https://doi.org/10.1016/0022-460X(71)90105-2.

Ho, C. M., and N. S. Nosseir. 1981. "Dynamics of an impinging jet. Part 1. The feedback phenomenon." *J. Fluid Mech.* 105 (Apr): 119–142. https://doi.org/10.1017/S0022112081003133.

Izdori, F., A. J. C. Semiao, and P. Perona. 2019. "The role of environmental variables in waste stabilization ponds' morphodynamics." *Front. Environ. Sci.* 7 (Nov): 159. https://doi.org/10.3389/fenvs.2019.00159.

Kegerise, M. A. 1999. "An experimental investigation of flow-induced cavity oscillations." Ph.D. thesis, Dept. of Mechanical and Aerospace Engineering, Syracuse Univ.

Lakzian, E., H. Saghi, and O. Kooshki. 2020. "Numerical simulation of sediment deposition and trapping efficiency estimation in settling basins, considering secondary flows." *Int. J. Sediment Res.* 35 (4): 347–354. https://doi.org/10.1016/j.ijsrc.2020.02.001.

Lamb, H. 1945. *Hydrodynamics*. New York: Cambridge University Press.

Larchevêque, L., P. Sagaut, I. Mary, O. Labbé, and P. Comte. 2003. "Large-eddy simulation of a compressible flow past a deep cavity." *Phys. Fluids* 15 (1): 193–210. https://doi.org/10.1063/1.1522379.

Li, H., and J. Sansalone. 2021. "CFD with evolutionary optimization for stormwater basin retrofits." *J. Environ. Eng.* 147 (7): 04021017. https://doi.org/10.1061/(ASCE)EE.1943-7870.0001881.

Liu, X., H. Xue, Z. Hua, Q. Yao, and J. Hu. 2013. "Inverse calculation model for optimal design of rectangular sedimentation tanks." *J. Environ. Eng.* 139 (Apr): 455–459. https://doi.org/10.1061/(ASCE)EE.1943-7870.0000655.

Mercier, B., T. Castelain, and C. Bailly. 2017. "Experimental characterisation of the screech feedback loop in underexpanded round jets." *J. Fluid Mech.* 824 (Jun): 202–229. https://doi.org/10.1017/jfm.2017.336.

Miozzi, M., and G. P. Romano. 2020. "Propagation of perturbations and meandering in a free surface shallow water jet." *Exp. Fluids* 61 (Apr): 1–18. https://doi.org/10.1007/s00348-020-03025-2.

Panda, J. 1999. "An experimental investigation of screech noise generation." *J. Fluid Mech.* 378 (Sep): 71–96. https://doi.org/10.1017/S0022112098003383.

Peltier, Y., S. Erpicum, P. Archambeau, M. Pirotton, and B. Dewals. 2014a. "Experimental investigation of meandering jets in shallow reservoirs."

Environ. Fluid Mech. 14 (3): 699–710. https://doi.org/10.1007/s10652-014-9339-2.

Peltier, Y., S. Erpicum, P. Archambeau, M. Pirotton, and B. Dewals. 2014b. "Meandering jets in shallow rectangular reservoirs: POD analysis and identification of coherent structures." *Exp. Fluids* 55 (Apr): 1–16. https://doi.org/10.1007/s00348-014-1740-6.

Peltier, Y., S. Erpicum, P. Archambeau, M. Pirotton, and B. Dewals. 2015. "Can meandering flows in shallow rectangular reservoirs be modeled with the 2D shallow water equations?" *J. Hydraul. Eng.* 141 (Mar): 04015008. https://doi.org/10.1061/(ASCE)HY.1943-7900.0001006.

Perrot-Minot, C., E. Mignot, R. Perkins, D. Lopez, and N. Riviere. 2020. "Vortex shedding frequency in open-channel lateral cavity." *J. Fluid Mech.* 892 (Nov): A25. https://doi.org/10.1017/jfm.2020.186.

Persson, J., and H. B. Wittgren. 2003. "How hydrological and hydraulic conditions affect performance of ponds." *Ecol. Eng.* 21 (4–5): 259–269. https://doi.org/10.1016/j.ecoleng.2003.12.004.

Powell, A., Y. Umeda, and R. Ishii. 1992. "Observations of the oscillation modes of choked circular jets." *J. Acoust. Soc. Am.* 92 (5): 2823–2836. https://doi.org/10.1121/1.404398.

Rabinovich, A. B. 2009. "Seiches and harbor oscillations." In *Handbook of coastal and ocean engineering*, 193–236. Singapore: World Scientific.

Rossiter, J. E. 1964. *Wind-tunnel experiments on the flow over rectangular cavities at subsonic and transonic speeds*. Aeronautical Research Council Reports and Memoranda, Tech. Rep. 3438. London: Stationery Office.

Rowley, C. W., D. R. Williams, T. Colonius, R. M. Murray, and D. G. Macmynowski. 2006. "Linear models for control of cavity flow oscillations." *J. Fluid Mech.* 547 (Jan): 317–330. https://doi.org/10.1017/S0022112005007299.

Tam, C. K., J. M. Seiner, and J. C. Yu. 1986. "Proposed relationship between broadband shock associated noise and screech tones." *J. Sound Vib.* 110 (2): 309–321. https://doi.org/10.1016/S0022-460X(86)80212-7.

Tarpagkou, R., and A. Pantokratoras. 2013. "CFD methodology for sedimentation tanks: The effect of secondary phase on fluid phase using DPM coupled calculations." *Appl. Math. Modell.* 37 (5): 3478–3494. https://doi.org/10.1016/j.apm.2012.08.011.

Yan, H., N. Vosswinkel, S. Ebbert, G. Lipeme Kouyi, R. Mohn, M. Uhl, and J.-L. Bertrand-Krajewski. 2020. "Numerical investigation of particles' transport, deposition and resuspension under unsteady conditions in constructed stormwater ponds." *Environ. Sci. Eur.* 32 (Dec): 1–17. https://doi.org/10.1186/s12302-020-00349-y.

Zhang, J.-M., H. P. Lee, B. C. Khoo, K. Q. Peng, L. Zhong, C.-W. Kang, and T. Ba. 2014. "Shape effect on mixing and age distributions in service reservoirs." *J. Am. Water Works Assoc.* 106 (Apr): E481–E491. https://doi.org/10.5942/jawwa.2014.106.0094.